A Finite Element Model for Investigating the Thermo-Electro-Mechanical Response of Inhomogeneously Deforming Dielectric Elastomer Actuators

Atul Kumar Sharma[1,*], Aman Khurana[2]
and Manish M. Joglekar[2]

[1]*Department of Mechanical Engineering, Indian Institute of Technology Jodhpur, Jodhpur 342037, India*
[2]*Department of Mechanical and Industrial Engineering, Indian Institute of Technology Roorkee, Roorkee 247667, India*
E-mail: atulksharma@iitj.ac.in
[*]*Corresponding Author*

Received 12 July 2021; Accepted 04 November 2021;
Publication 26 November 2021

Abstract

Among the available soft active materials, Dielectric elastomers (DEs) possess the capability of achieving the large actuation strain under the application of high electric field. The material behavior of such elastomers is affected significantly by the change in temperature. This paper reports a 3-D finite element framework based on the coupled nonlinear theory of thermo-electro-elasticity for investigating the thermal effects on the electromechanical performance of inhomogeneously deforming dielectric elastomer actuators (DEAs). The material behavior of the actuator is modeled using the neo-Hookean model of hyperelasticity with temperature dependent shear modulus. An in-house computational code is developed to implement the coupled finite element framework. Firstly, the accuracy of the developed FE code

European Journal of Computational Mechanics, Vol. 30_4–6, 387–408.
doi: 10.13052/ejcm2642-2085.30464

is verified by simulating the temperature effects on the actuation response and pull-in instability of the benchmark homogeneously deforming planar DE actuator. Further, the influence of temperature on the electromechanical responses of complex bi-layered bending actuator and buckling pump actuator involving inhomogeneous deformation is investigated. The numerical framework and the associated inferences can find their potential use in addressing the effect of temperature in the design of electro-active polymer based actuators.

Keywords: Dielectric elastomers, nonlinear thermo-electro-hyperelasticity, finite element method, finite deformation, inhomogeneous deformation, buckling pump actuator.

1 Introduction

Dielectric elastomers a unique group of electroactive-polymers (EAPs) exhibit an exceptional property of undergoing large elastic deformations in response to electric stimulation. Because of their large actuation strain, high energy density, high coupling efficiency, etc., DEs have become one of the most potentially used materials in recent years [1]. Due to these unique characteristics, the DEs are effectively used in energy harvesting devices, peristaltic pumps, soft grippers, artificial muscles, adjustable noise reduction system in aeroplanes, actuators, adaptable valves in car engines, minimum energy structures, among the others [2–6].

Three types of polymers are used prevalently in EAPs/DE applications; they are acrylics, polyurethanes, and silicones. While the silicone-based EAPs show less temperature sensitivity [7, 8]; in contrast, the acrylic-based EAPs are highly temperature sensitive [9–12]. There are several application examples, such as the DE-based soft robot deployed in the sea environment [6], adjustable noise reduction system in aeroplanes [3], and adaptable valves in car engines [4] wherein the DE actuators are subjected to a large variation in operating temperatures. In view of this, it is imperative to incorporate and analyse the effect of temperature in the analysis of DE actuators for facilitating an efficient design.

In the recent past, many researchers have reported the lumped parameter models pertaining to DEAs considering the temperature effects [11–15]. In context to lumped parameter modeling of DEs, Sheng et al. [14] presented a parametric study for exploring the influence of deformation-dependent

permittivity and temperature on the electromechanical instability of DEs in the quasi-static mode of operation. Liu et al. [15] presented a constitutive model of the thermodynamic system based on the adiabatic process to study the thermo-electromechanical stability of DEs. Chen et al. [11] presented an analytical model for analyzing the temperature effects on the actuation behavior and modes of failure of a dissipative dielectric elastomer actuator. Further, Sheng et al. [16] investigated the thermal effects on the nonlinear dynamic behavior of viscoelastic DEAs by implementing a temperature dependent dielectric constant model. Vertechy et al. [17] presented an experimentally corroborated coupled thermo-electro-elastic continuum model for analyzing homogeneously deforming isotropic modified-entropic hyperelastic elastomers subjected to combined thermo-electro-mechanical loading. Kleo et al. [12] presented the theoretical and experimental investigations to determine the electromechanical breakdown strength and behavior of DEs by considering the effect of temperature and strain-stiffening. In almost all of the aforementioned models, the researchers have their attention centered on simple unconstrained configurations of DEAs (i.e., planar actuators) deforming homogeneously. However, in actual practice, DE based actuators (i.e., Bending actuators, buckling pump actuators, and many others) undergo inhomogeneous deformations and for investigating their thermo-electro-mechanical behavior an appropriate numerical framework is needed.

To this end, in this paper, a finite element-based numerical framework is reported for investigating the thermal effects on the electromechanical performance of inhomogeneously deforming dielectric elastomers. The utility of the developed finite element model is demonstrated by assessing the effect of temperature on the pull-in instability phenomena of homogeneously deforming DEAs, and further used to study a few case studies of practical importance, such as bi-layered bending and buckling pump actuators involving inhomogeneous deformations.

The remainder of the paper is organized as follows. Section 2 summarizes the governing equations pertaining to the finite strain nonlinear thermo-electro-mechanical deformation of dielectric elastomers following the general theory of nonlinear thermo-electro-elasticity [18]. The finite element model for the coupled thermo-electro-elastic problem is presented in Section 3. In Section 4, we consider three problems to demonstrate the capability of the finite element model in capturing the nonlinear thermo-electro-mechanical response of DEs. Concluding remarks are provided in Section 5.

2 Overview of the Nonlinear Thermo-Electro-Mechanics

Consider a continuum dielectric body $\mathcal{B}_0$ in the reference configuration at time $t = 0$, with boundary $\partial\mathcal{B}_0$ and a material point having position vector X_J as shown in Figure 1. At time $t > 0$, due to thermo-electro-mechanical loading, material point X_J moves to a point $x_i(X_J, t)$ in the current configuration of the body $\mathcal{B}_t$ with boundary $\partial\mathcal{B}_t$. The absolute temperature of the material point X_J at time $t = 0$ and $t > 0$ are denoted by θ_0 and $\theta(X_J, t)$, respectively. The electric potential corresponding to the material point X_J is denoted by $\phi(X_J, t)$. We define the deformation gradient as $F_{iJ}(X_J, t) = \partial x_i(X_J, t)/\partial X_J$ with Jacobian $J = det(F) > 0$, and the electric field as $E_J = -\partial\phi(X_J, t)/\partial X_J$ in the reference state with Faraday's law of electrostatics $(\partial E_J/\partial X_K)\grave{o}_{IJK} = 0$. The right Cauchy-Green strain tensor is defined as $C_{IJ} = F_{KI}F_{KJ}$. Let, $\mathcal{B}_\theta$ represents the intermediate state of the dielectric body and its associated boundary is represented by $\partial\mathcal{B}_\theta$. Following [19, 20], to take into account thermal effects, we introduce the multiplicative decomposition of the total deformation gradient into two parts as

$$F_{iJ} = F^{EM}_{ik} F^{\theta}_{kJ}, \tag{1}$$

where, F^{EM}_{ik} and F^{θ}_{kJ} denotes the electro-mechanical and thermal components of the deformation gradient, respectively. We consider the thermal part of the deformation gradient as pure volumetric contribution $F^{\theta}_{kJ} = J^{\theta^{1/3}}\delta_{kJ}$, with determinant $J^\theta = \exp(3\alpha(\theta - \theta_0))$ [21]. Here, α is the

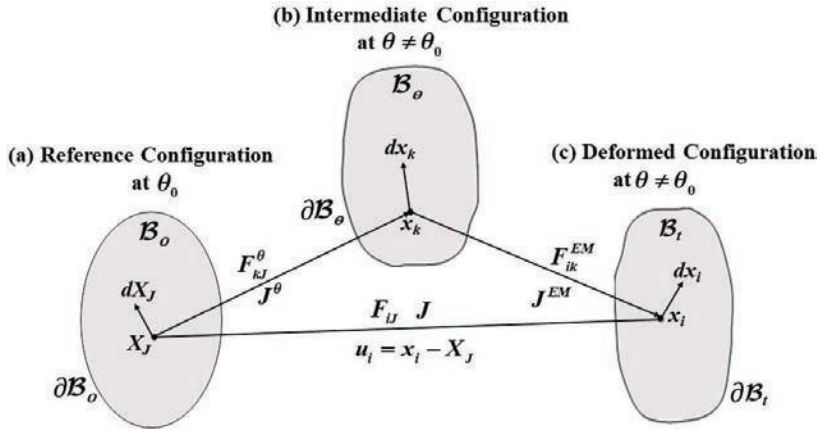

Figure 1 An arbitrary continuum dielectric body in the (a) reference configuration, (b) intermediate configuration, and (c) deformed configuration.

coefficient of thermal expansion. By utilizing the aforementioned relations and Equation (1), electro-mechanical components of deformation gradient (F_{ik}^{EM}), Cauchy-Green strain tensor (C_{IJ}^{EM}), and Jacobian (J^{EM}) are written in terms of J^{θ} as

$$F_{ik}^{EM} = J^{\theta^{-1/3}} F_{ik}; \quad C_{IJ}^{EM} = J^{\theta^{-2/3}} C_{IJ}; \quad J^{EM} = J/J^{\theta}. \tag{2}$$

Neglecting inertial effects and electrodynamic effects, the balance of linear momentum of dielectric body and Gauss's law in the reference configuration are expressed as

$$\frac{\partial P_{iJ}}{\partial X_J} + \bar{b}_i = 0; \quad \frac{\partial D_J}{\partial X_J} = \bar{q}; \quad \text{in } \mathcal{B}_0 \tag{3}$$

respectively, where $P_{iJ} = F_{iI} S_{IJ}$ is the first Piola-Kirchhoff stress tensor (PK-1), S_{IJ} is the second Piola-Kirchhoff stress tensor (PK-2), D_J is the electric displacement vector, $\bar{q}$ and $\bar{b}_i$ are the free charge density and an external body force density vector in the reference configuration, respectively. The Neumann boundary conditions for P_{iJ} and D_J, and Dirichlet boundary conditions for displacement u_i and electric potential ϕ are defined as

$$\begin{aligned} &\bar{t}_i = P_{iJ} N_J \quad \text{on} \quad \partial\mathcal{B}_0^{\bar{t}}; \quad \bar{\omega} = -D_J N_J \quad \text{on} \quad \partial\mathcal{B}_0^{\bar{\omega}}; \\ &u_i = \bar{u}_i \quad \text{on} \quad \partial\mathcal{B}_0^{\bar{u}}; \quad \phi = \bar{\phi} \quad \text{on} \quad \partial\mathcal{B}_0^{\bar{\phi}}; \end{aligned} \tag{4}$$

where $\bar{t}_i$ and $\bar{\omega}$ are the prescribed traction vector and surface charge density on the Neumann parts $\partial\mathcal{B}_0^{\bar{t}}$ and $\partial\mathcal{B}_0^{\bar{\omega}}$ of the boundary $\partial\mathcal{B}_0$, respectively, N_J represents an outward unit normal on the Neumann surface, $\bar{u}_i$ and $\bar{\phi}$ are the prescribed displacement vector and electric potential on the Dirichlet parts $\partial\mathcal{B}_0^{\bar{u}}$ and $\partial\mathcal{B}_0^{\bar{\phi}}$ of the boundary $\partial\mathcal{B}_0$. The thermal field equation obtained from the first law of thermodynamics and corresponding boundary conditions can be expressed as

$$\begin{aligned} &\theta\dot{\eta} = -\frac{\partial Q_J}{\partial X_J} + R \quad \text{in} \quad \mathcal{B}_0, \\ &\bar{Q} = Q_J N_J \quad \text{on} \quad \partial\mathcal{B}_{\theta}^{\bar{Q}}; \quad \theta = \bar{\theta} \quad \text{on} \quad \partial\mathcal{B}_{\theta}^{\bar{\theta}}, \end{aligned} \tag{5}$$

where, η represents the entropy, Q_J is the heat flux vector, and *R* represents a volumetrically distributed heat source in the material configuration, $\bar{Q}$ represents the prescribed heat flux on the Neumann part $\partial\mathcal{B}_{\theta}^{\bar{Q}}$ associated

with the boundary $\partial\mathcal{B}_\theta$ and $\bar{\theta}$ shows prescribed absolute temperature on the Dirichlet part $\partial\mathcal{B}_\theta^{\bar{\theta}}$ associated with the boundary $\partial\mathcal{B}_\theta$.

We consider non-dissipative, ideal dielectric material model neglecting the effect of time dependent viscoelasticity for which PK-2 stress S_{IJ}, electric displacement D_J, and entropy η are obtained constitutively through an augmented energy density function $\psi(C, E, \theta)$ as [12, 17]

$$S_{IJ} = 2\frac{\partial\psi}{\partial C_{IJ}}; \quad D_J = -\frac{\partial\psi}{\partial E_J}; \quad \eta = -\frac{\partial\psi}{\partial\theta}. \tag{6}$$

We specify the following form of the thermo-electromechanically coupled augmented free energy density function to characterize the constitutive behaviour of the dielectric elastomers [13, 22]:

$$\begin{aligned}\psi(C,E,\theta) = \frac{\theta}{\theta_0}\left[\frac{\mu(\theta)}{2}\{C_{PP}^{EM} - 3 - 2\ln(J^{EM})\} + \frac{K}{2}\ln^2(J^{EM})\right] \\ - \frac{\varepsilon}{2}JC_{PQ}^{-1}E_PE_Q - c\left[\theta - \theta_0 - \theta\ln\left(\frac{\theta}{\theta_0}\right)\right] \\ - 3\alpha K(\theta-\theta_0)\frac{\ln(J_\theta)}{J_\theta},\end{aligned} \tag{7}$$

where, μ and K are the shear and bulk modulus, respectively, ε is the dielectric permittivity, and c is the specific heat capacity. Substituting Equation (7) into Equation (6), we obtain the following constitutive relations

$$D_J = \varepsilon JC_{JQ}^{-1}E_Q, \tag{8}$$

$$\begin{aligned}P_{iJ} = \frac{\theta}{\theta_0}\begin{bmatrix}\mu(\theta)\{(J_\theta)^{-2/3}\delta_{IJ} - C_{IJ}^{-1}\} \\ + K\ln(J^{EM})C_{IJ}^{-1}\end{bmatrix}F_{iI} \\ + \varepsilon JE_PE_Q\left(C_{PI}^{-1}C_{JQ}^{-1} - \frac{1}{2}C_{IJ}^{-1}C_{PQ}^{-1}\right)F_{iI},\end{aligned} \tag{9}$$

$$\begin{aligned}\eta = -\frac{1}{\theta_0}\left[\frac{\mu(\theta)}{2}\{C_{PP}^{EM} - 3 - 2\ln(J^{EM})\} + \frac{K}{2}\ln^2(J^{EM})\right] \\ - \frac{\theta}{\theta_0}\left[\frac{\mu(\theta)}{2}\{6\alpha - 2\alpha C_{PP}^{EM}\} - 3\alpha K\ln(J^{EM})\right] - c\ln\left(\frac{\theta}{\theta_0}\right) \\ - 3\alpha K\frac{\ln(J_\theta)}{J_\theta} - 3\alpha^2K(\theta-\theta_0)\left(\frac{1-\ln(J_\theta)}{J_\theta}\right).\end{aligned} \tag{10}$$

The expression for the heat flux vector Q_J which satisfies the inequality of heat conduction via isotropic Fourier model of heat conduction takes the following form [23]

$$Q_J = -kJC_{JP}^{-1}\theta'_p, \tag{11}$$

where, k denotes the isotropic thermal conductivity and $\theta'_p = \partial\theta/\partial X_P$ represents the temperature gradient. Moreover, by utilizing the free energy function ψ, its total time derivative and constitutive equations, we express the rate of entropy as

$$\dot{\eta} = c\frac{\dot{\theta}}{\theta} - \frac{\partial P_{iJ}}{\partial\theta}\dot{F}_{iJ} - \frac{\partial D_J}{\partial\theta}\dot{E}_J. \tag{12}$$

On substitution of the expression of the rate of entropy from Equation (12) into Equation (5), governing thermal field equation can be formulated as the equation of heat conduction as

$$c\dot{\theta} = -\frac{\partial Q_I}{\partial X_I} + R + H = 0, \tag{13}$$

where,

$$H = \theta\frac{\partial P_{iJ}}{\partial\theta}\dot{F}_{iJ} - \theta\frac{\partial D_J}{\partial\theta}\dot{E}_J.$$

3 Finite Element Framework

The solution of the governing partial differential Equations (3) and (13) using the finite element method requires their weak forms. At time t_n, the weak forms of the governing differential equations obtained by contracting the equation of momentum balance equation with virtual displacement vector δu_i, the Gauss law equation by the virtual electric potential $\delta\phi$, and heat equation with virtual temperature $\delta\theta$ and integrating over the entire volume in the reference state, are expressed as

$$r^u = \underbrace{\int_{\mathcal{B}_0} P_{iJ}\frac{\partial\delta u_i}{\partial X_J}dV}_{r^u_{\text{int}}} \underbrace{- \int_{\partial\mathcal{B}_0} \bar{t}_i\delta u_i dA - \int_{\partial\mathcal{B}_0} \bar{b}_i\delta u_i dV}_{r^u_{\text{ext}}} = 0, \tag{14a}$$

$$r^\phi = \underbrace{\int_{\mathcal{B}_0} D_J\frac{\partial N_a}{\partial X_J}dV}_{r^\phi_{\text{int}}} \underbrace{+ \int_{\partial\mathcal{B}_0} \bar{\omega}N_a dA + \int_{\mathcal{B}_0} \bar{q}N_a dV}_{r^\phi_{\text{ext}}} = 0, \tag{14b}$$

$$r^{\theta} = \underbrace{\int_{\mathcal{B}_0} c\dot{\theta}\delta\theta dV - \int_{\mathcal{B}_0} Q_J \frac{\partial \delta\theta}{\partial X_J} dV}_{r^{\theta}_{\text{int}}}$$

$$\underbrace{- \int_{\partial\mathcal{B}_0} (H+R)\delta\theta dA - \int_{\mathcal{B}_0} \bar{Q}\delta\theta dV}_{r^{\theta}_{\text{ext}}} = 0, \tag{14c}$$

where $(\bullet)_{\text{int}}$, and $(\bullet)_{\text{ext}}$ represent the internal and external force vectors, respectively. We use an implicit backward-Euler scheme for approximating the time derivative of temperature present in Equation 14(c) as $\dot{\theta} = (\theta_n - \theta_{n-1})/\Delta t$, where θ_n and θ_{n-1} are the temperature fields at time t_n and t_{n-1}, and Δt is the time increment. Next, by considering the finite element approximations for the virtual displacement $\delta u_i = N_a \delta u_{ai}$, electric potential $\delta\phi = N_a \delta\phi_a$, virtual temperature $\delta\theta = N_a \delta\theta_a$, with N_a representing shape function associated with node a, δu_{ai}, $\delta\theta_a$, and $\delta\phi_a$ denoting the nodal virtual displacement vector, virtual temperature and virtual electric potential values, respectively. We obtain the following elemental level equations pertaining to mechanical, electrical, and thermal equilibrium at time t_n,

$$r^{u} = \int_{\mathcal{B}_0} P_{iJ} \frac{\partial N_a}{\partial X_J} dV - \int_{\partial\mathcal{B}_0} \bar{t}_i N_a dA - \int_{\mathcal{B}_0} \bar{b}_i N_a dV = 0, \tag{15}$$

$$r^{\phi} = \int_{\mathcal{B}_0} D_J \frac{\partial N_a}{\partial X_J} dV + \int_{\partial\mathcal{B}_0} \bar{\omega} N_a dA + \int_{\mathcal{B}_0} \bar{q} N_a dV = 0, \tag{16}$$

$$r^{\theta} = \int_{\mathcal{B}_0} c\dot{\theta} N_a dV - \int_{\mathcal{B}_0} Q_J \frac{\partial N_a}{\partial X_J} dV$$

$$- \int_{\partial\mathcal{B}_0} (H+R) N_a dA - \int_{\mathcal{B}_0} \bar{Q} N_a dA = 0. \tag{17}$$

We solve these coupled nonlinear Equations (15)–(17), using an incremental-iterative strategy based on Newton–Raphson approach and resulting incremental equations at time t_n and m^{th} Newton iteration are written as

$$K^{uu}|_m \, \Delta u_{bk} + K^{u\phi}|_m \, \Delta\phi_b + K^{u\theta}|_m \, \Delta\theta_b = -r^{u}|_m, \tag{18a}$$

$$K^{\phi u}|_m \, \Delta u_{bk} + K^{\phi\phi}|_m \, \Delta\phi_b = -r^{\phi}|_m, \tag{18b}$$

$$K^{\theta u}|_m \, \Delta u_{bk} + K^{\theta\theta}|_m \, \Delta\theta_b = -r^{\theta}|_m, \tag{18c}$$

where, the stiffness matrices are expressed as

$$K^{uu} = \int_{\mathcal{B}_0} \frac{\partial N_a}{\partial X_J} \frac{\partial P_{iJ}}{\partial F_{kL}} \frac{\partial N_b}{\partial X_L} dV; \quad K^{u\phi} = -\int_{\mathcal{B}_0} \frac{\partial N_a}{\partial X_J} \frac{\partial P_{iJ}}{\partial E_L} \frac{\partial N_b}{\partial X_L} dV;$$

$$K^{u\theta} = \int_{\mathcal{B}_0} \frac{\partial N_a}{\partial X_J} \frac{\partial P_{iJ}}{\partial \theta} N_b dV; \quad K^{\theta u} = -\int_{\mathcal{B}_0} \frac{\partial N_a}{\partial X_J} \frac{\partial Q_J}{\partial F_{kL}} \frac{\partial N_b}{\partial X_L} dV;$$

$$K^{\phi\phi} = -\int_{\mathcal{B}_0} \frac{\partial N_a}{\partial X_J} \frac{\partial D_J}{\partial E_L} \frac{\partial N_b}{\partial X_L} dV; \quad K^{\phi u} = \int_{\mathcal{B}_0} \frac{\partial N_a}{\partial X_J} \frac{\partial D_J}{\partial F_{kL}} \frac{\partial N_b}{\partial X_L} dV;$$

$$K^{\theta\theta} = \int_{\mathcal{B}_0} \frac{c}{\Delta t} N_a N_b dV - \int_{\mathcal{B}_0} \frac{\partial N_a}{\partial X_J} \frac{\partial Q_J}{\partial \theta_L} \frac{\partial N_b}{\partial X_L} dV. \tag{19}$$

The analytical expressions for different thermo-electro hyperelastic tangent moduli using Equations (8)–(9) and Equation (11) are written as

$$\begin{aligned}
\frac{\partial P_{iJ}}{\partial F_{kL}} = {} & \frac{\theta}{\theta_0}[\mu\{(J_\theta)^{-2/3}\delta_{JL}\delta_{iK} - C^{-1}_{JL}\delta_{iK}\} \\
& + K\ln(J^{EM})C^{-1}_{JL}\delta_{iK}] \\
& + \varepsilon J E_P E_Q \delta_{iK}\left(C^{-1}_{PJ}C^{-1}_{LQ} - \frac{1}{2}C^{-1}_{JL}C^{-1}_{PQ}\right) \\
& + \frac{\theta}{\theta_0}\begin{bmatrix} \mu(C^{-1}_{IK}C^{-1}_{JL} + C^{-1}_{IL}C^{-1}_{JK})F_{iI}F_{kK} + KC^{-1}_{IJ}C^{-1}_{KL}F_{iI}F_{kK} \\ -K\ln J^{EM}(C^{-1}_{IK}C^{-1}_{JL} + C^{-1}_{IL}C^{-1}_{JK})F_{iI}F_{kK} \end{bmatrix} \\
& + \varepsilon J E_P E_Q F_{iI}F_{kK}\begin{bmatrix} C^{-1}_{KL}\left(C^{-1}_{PI}C^{-1}_{JQ} - \frac{1}{2}C^{-1}_{IJ}C^{-1}_{PQ}\right) \\ + C^{-1}_{IJ}C^{-1}_{PK}C^{-1}_{QL} \\ + \frac{1}{2}C^{-1}_{PQ}(C^{-1}_{IK}C^{-1}_{JL} + C^{-1}_{IL}C^{-1}_{JK}) \end{bmatrix} \\
& - \varepsilon J E_P E_Q F_{iI}F_{kK}\begin{bmatrix} C^{-1}_{PI}(C^{-1}_{JK}C^{-1}_{QL} + C^{-1}_{JL}C^{-1}_{QK}) \\ -C^{-1}_{JQ}(C^{-1}_{PK}C^{-1}_{IL} + C^{-1}_{PL}C^{-1}_{IK}) \end{bmatrix},
\end{aligned} \tag{20}$$

$$\frac{\partial P_{iJ}}{\partial E_L} = \varepsilon J E_Q[C^{-1}_{LI}C^{-1}_{QJ} + C^{-1}_{QI}C^{-1}_{LJ} - C^{-1}_{LQ}C^{-1}_{IJ}]F_{iI}, \tag{21}$$

$$\frac{\partial P_{iJ}}{\partial \theta} = \frac{1}{\theta_0}[\mu\{(J_\theta)^{-2/3}\delta_{IJ} - C_{IJ}^{-1}\} + K\ln(J^{EM})C_{IJ}^{-1}]F_{iI}$$

$$- \frac{\theta}{\theta_0}[2\mu\alpha(J_\theta)^{-2/3}\delta_{IJ} + 3\alpha K C_{IJ}^{-1}]F_{iI}, \tag{22}$$

$$\frac{\partial D_J}{\partial F_{kL}} = \varepsilon J E_Q[C_{JQ}^{-1}C_{KL}^{-1} - C_{JK}^{-1}C_{QL}^{-1} - C_{JL}^{-1}C_{QK}^{-1}]F_{kK}, \tag{23}$$

$$\frac{\partial D_J}{\partial E_L} = \varepsilon J C_{JL}^{-1}; \quad \frac{\partial Q_J}{\partial \theta'_L} = -kJC_{JL}^{-1}, \tag{24}$$

$$\frac{\partial Q_J}{\partial F_{kL}} = kJ\theta'_P[C_{JK}^{-1}C_{PL}^{-1} + C_{JL}^{-1}C_{PK}^{-1} - C_{JP}^{-1}C_{KL}^{-1}]F_{kK}. \tag{25}$$

4 Numerical Results

To demonstrate the capability of the aforementioned finite element framework, we consider three different problems pertaining to the thermo-electromechanical behavior of soft DE actuators. The specific problems are thermal effects on the pull-in instability of a planar actuator and the electromechanical responses of inhomogeneously deforming bending and buckling pump actuators. We use a standard 8-noded linear hexahedral solid element with a selective reduced integration scheme [24–26]. This choice, together with a high value of bulk modulus (10^3 times the shear modulus) ensures adequate handling of material incompressibility in the analysis. The temperature dependent shear moduli of the DE actuator is defined as $\mu(\theta) = \frac{1}{3}[A(\frac{1000}{\theta})^2 + B(\frac{1000}{\theta}) + C]$ with $A = 0.2001$, $B = -1.078$ and $C = 1.5180$, for five different feasible temperature $\theta = 273$, 293, 313, 333 and 353K [27] is incorporated to vary the shear modulus of the actuator as depicted in Figure 2. The material parameters used in all problems are listed in Table 1 [13, 18, 25].

4.1 Validation of the Finite Element Model: Homogeneously Deforming Planar Dielectric Elastomer Actuator

For the verification of the finite element framework, we simulate the temperature effects on the well-known pull-in instability of a planar DE actuator. In this configuration, an unconstrained DE film is sandwiched between two compliant electrodes on both sides. When driven by the potential difference between the two electrodes, the DE film is compressed in the thickness

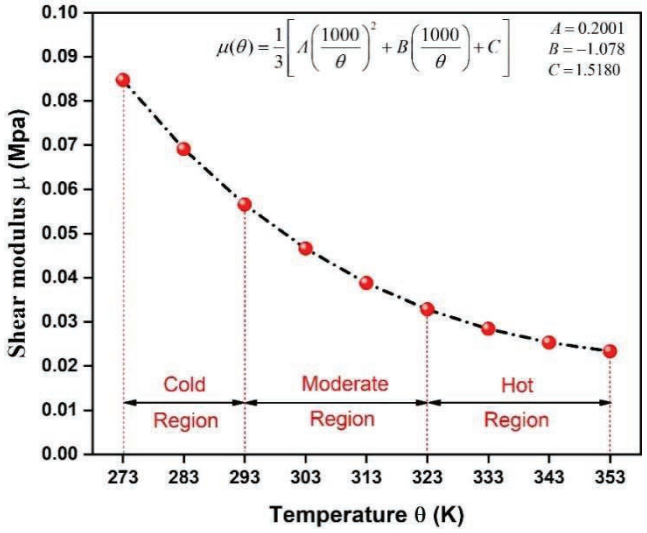

Figure 2 Variation of shear moduli of the dielectric elastomer with temperature.

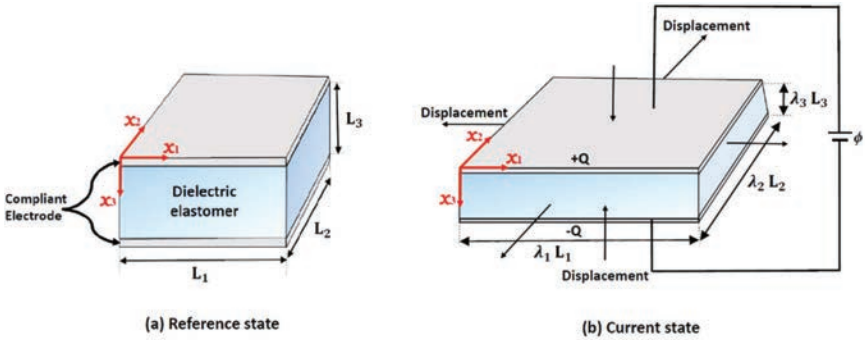

Figure 3 A schematic of a homogeneously deforming planar dielectric elastomer actuator in the (a) reference state at temperature θ_0, and in the (b) current state at temperature θ and subjected to potential difference ϕ.

direction and expands laterally. A positive feedback between the thickness reduction and the concomitant increment of the electric field results in an operational instability referred to as the pull-in instability [15, 28–31]. Figure 3 depicts the schematic of a planar dielectric elastomer in the reference state (reference temperature θ_0) and in the current state, when subjected to electric potential difference ϕ in the x_3-direction and the temperature is raised to θ. The stretch ratio of the actuator in the i^{th} principal direction is defined as

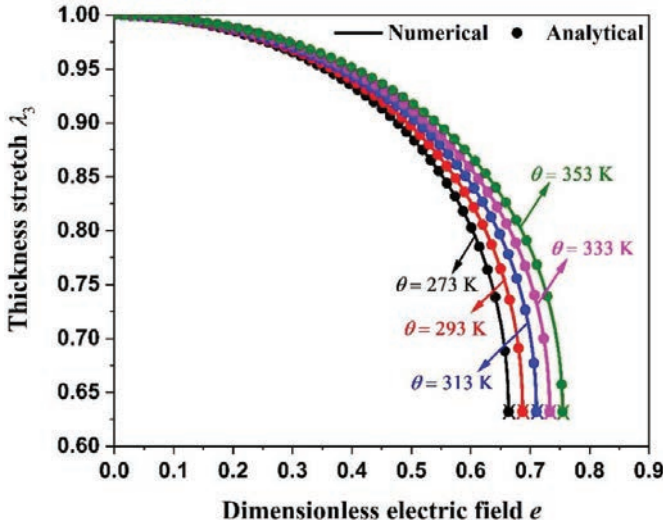

Figure 4 Comparison of the numerical values of principal thickness stretch (λ_3) versus dimensionless electric field, (e) at five different temperatures: $\theta = 273$, 293, 313, 333 and 353 K with the previously reported analytical solution [13].

$\lambda_i = l_i/L_i$, where l_i and L_i denote the i^{th} principal dimension of the actuator in the current and reference states, respectively. In numerical simulations, the geometry of the actuator (having dimensions: $L_1 = L_2 = 5$ mm, $L_3 = 1$ mm) is discretized using 8 hexahedral elements. We impose the following symmetric displacement boundary conditions: the nodes at the surfaces $x_1 = 0$, $x_2 = 0$, and $x_3 = 0$ are restricted to move along the x_1, x_2 and x_3 directions, respectively. We monotonically increase the electric potential difference ϕ between the surfaces $x_3 = 0$ and $x_3 = L_3$ until the pull-in instability takes place. We specify the following constant temperature boundary conditions: (1) $\theta = \theta_0$ at the surfaces $x_3 = 0$ and $x_3 = L_3$, for time $t = 0$, (2) $\theta = \bar{\theta}$ at the surfaces $x_3 = 0$ and $x_3 = L_3$, for time $t > 0$. The reference temperature θ_0 is taken to 293 K (room temperature) [27].

Figure 4 shows the comparison of the numerically simulated thickness stretch λ_3 Vs the non-dimensional electric field $e = \frac{\phi}{L_3}\sqrt{\frac{\varepsilon}{\mu}}$ response of the actuator with the analytical model reported by Sheng et al. [13] for obtaining the electromechanical instability (EMI) state. Figure 4 shows an excellent match between the analytical predictions and those obtained numerically, thus ascertaining the accuracy and capability of the presented FE framework of predicting the thermal effects on the electromechanical behavior of DEs. It

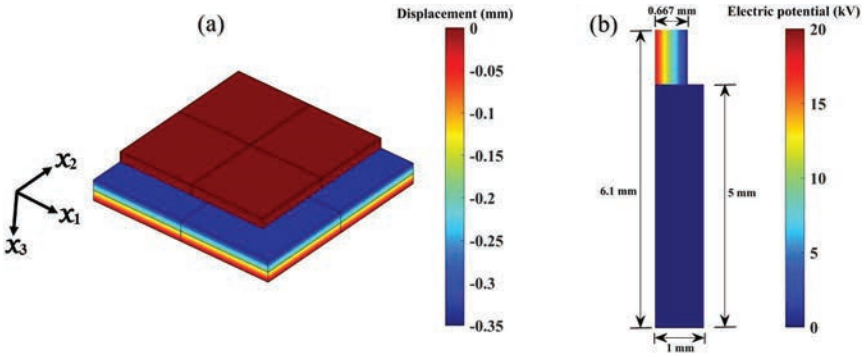

Figure 5 Deformed and undeformed configurations of the planar actuator, (a) with a displacement plot along the thickness (u_3) in mm, and (b) in $x_2 - x_3$ plane showing the electric potential distribution plot ϕ in kV, of dielectric elastomer at 18.2 kV and temperature 353 K.

should however be noted that the pull-in parameters (critical field and stretch) would depend strongly upon the choice of the material and the boundary conditions. From Figure 4, it is observed that as the temperature increases, the dimensionless electric-field (e) at the onset of pull-in instability [Marked by **X** symbol] also increases. This figure also shows that the level of deformation at the instability point is independent of level of temperature. Figures 5(a) and 5(b) depict the undeformed and deformed configurations of the dielectric block at $\theta = 353$ K, $\phi = 18.2$ kV, with the plots of displacement in the thickness directions and electric potential distributions, respectively.

4.2 Bi-layered Bending Actuator

Our second problem comprises the temperature effect on the electromechanical behavior of a bi-layered bending actuator consisting of two perfectly bonded active and passive layers as shown in Figure 6(a). The geometrical parameters of the actuator are selected as length $(L) = 20$ mm, width $(W) = 4$ mm and thickness $(H) = 1$ mm. The actuator is discretized with 20, 8, and 4 hexahedral elements along the length, width, and thickness, respectively (see Figure 6(b)).

The boundary conditions are specified as: all nodes corresponding to the surface $a'b'd'c'$ ($x_3 = 0$) are restricted along the x_3 direction, the surfaces $a'c'ca$ ($x_2 = 0$) and $b'd'db$ ($x_2 = W$) cannot move in the x_2 direction, and the nodes at the intersection of surfaces $x_1 = H$ and $x_3 = 0$ are confined along the x_1 direction. The electrical boundary conditions are specified by setting $\phi = 0$ on the surface $x_1 = H$ and monotonically increasing voltage ϕ on the

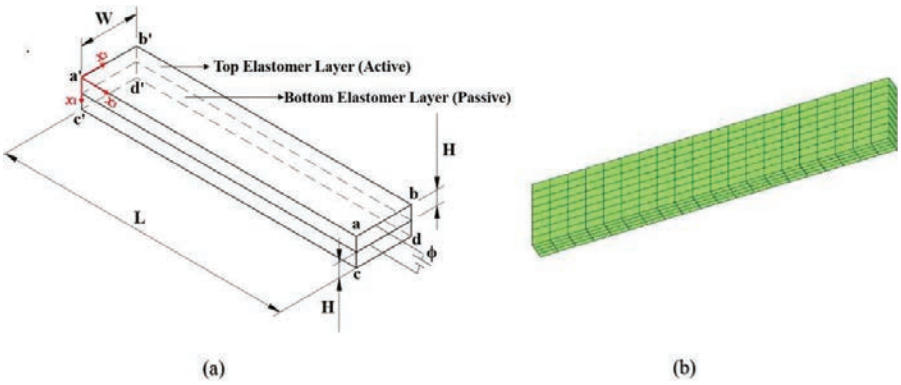

Figure 6 (a) A schematic of a Bi-layered bending actuator, and (b) finite element mesh.

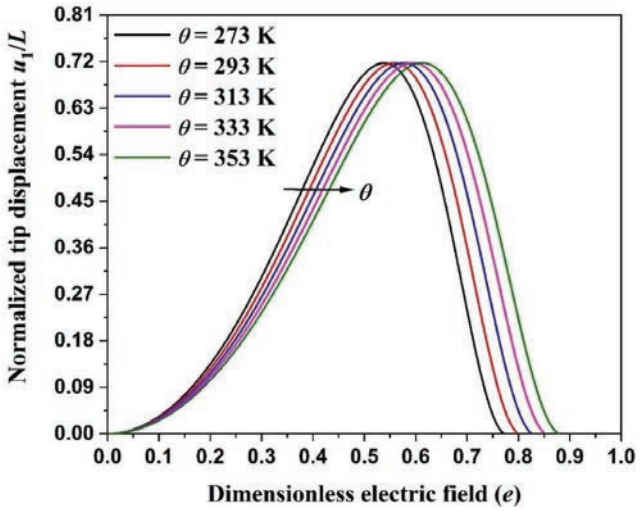

Figure 7 Numerically simulated normalized tip deflection Vs dimensionless electric field curves for five different temperatures: $\theta = 273$, 293, 313, 333 and 353 K.

surface $x_1 = 0$ until the actuator undergoes almost 360 deg. angle bend. We impose the following temperature boundary conditions on the surfaces $a'b'ba$ ($x_1 = 0$) and $c'd'dc$ ($x_1 = 2H$): (1) $\theta = \theta_0$ for time $t = 0$, and (2) $\theta = \bar{\theta}$ for time $t > 0$.

Figure 7 shows the normalized tip deflection of the actuator with respect to the dimensionless electric field $e = \frac{2\phi}{H}\sqrt{\frac{\varepsilon}{\mu}}$ for five different levels of the temperature $\theta = 273$, 293, 313, 333, and 353 K. From this figure, we notice

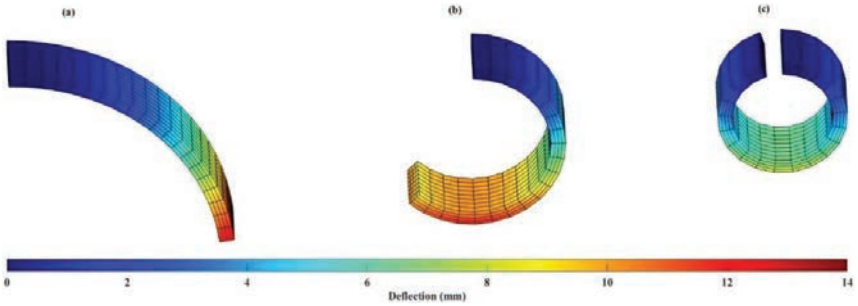

Figure 8 Deformed configurations of a bi-layered bending actuator with a color plot of the deflection (u_1) in mm at different values of applied dimensionless electric field e (a) 0.5, (b) 0.75, and (c) 0.87, and temperature $\theta = 353$ K.

that the level of deformation (u_1/L) of the bending actuator increases with a decrease in the temperature, for any value of the applied electric field. Figures 8(a–c) demonstrate the deformed configurations of the bending actuator (at 353 K temperature field) along with displacement contour plots for the applied dimensionless electric field equal to 0.5, 0.75, and 0.87, respectively. From Figure 8(c), we observe complete (almost 360 deg.) bending of the actuator, when applied dimensionless electric field is equal to 0.87.

4.3 Buckling Pump Actuator

Our final problem considers the temperature effects on the DEs based peristaltic buckling pump involving inhomogeneous deformation while transferring fluids [2, 25, 32]. Figure 9, shows the schematic of a DE based buckling pump actuator consisting of two unbonded layers of DE fixed at the ends. In the numerical simulation, the dimensions of both the layers are same with length $(L) = 20$ mm, width $(W) = 4$ mm, and thickness $(H) = 1$ mm. Each layer of the pump is modeled with 4, 8, and 20 hexahedron elements along the x_1, x_2, and x_3 directions, respectively. The boundary conditions are specified as: The nodes corresponding to the surfaces $a'b'd'c'$ ($x_3 = 0$) and $abdc$ ($x_3 = L$) are restricted along all the three directions, the voltage is zero on the interface between the upper and lower layers and we monotonically increase voltage on the surfaces $x_1 = 0$ and $x_1 = 2H$ until the pump actuator buckles. The temperature of the surfaces $a'b'ba$ ($x_1 = 0$) and $c'd'dc$ ($x_1 = 2H$) is defined as (1) $\theta = \theta_0$ for time $t = 0$, and (2) $\theta = \bar{\theta}$ for time $t > 0$. Figure 10 depicts the normalized central deflection of the pump actuator with respect to the dimensionless electric field $e = \frac{\phi}{H}\sqrt{\frac{\varepsilon}{\mu}}$ for the

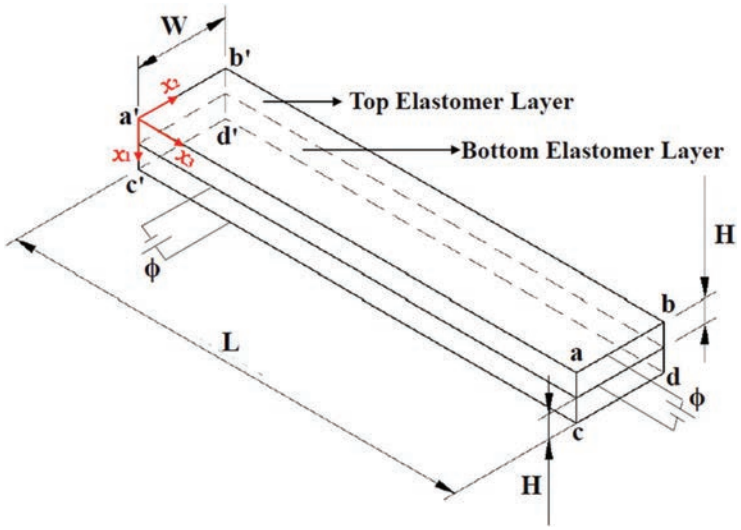

Figure 9 A schematic of a buckling pump actuator.

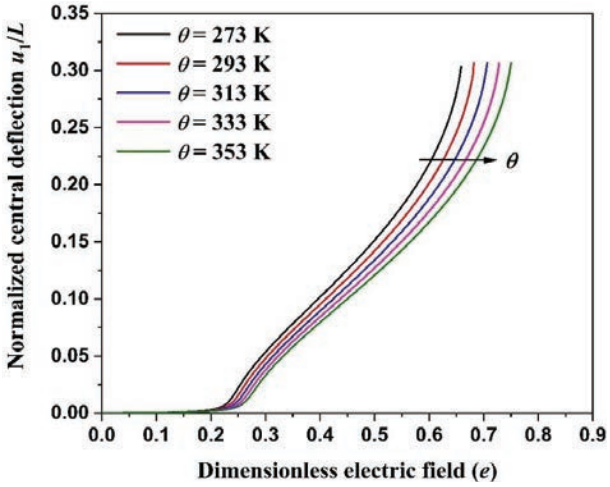

Figure 10 Normalized central deflection Vs dimensionless electric field curves for buckling pump actuator at five different temperatures: $\theta = 273$, 293, 313, 333, and 353 K.

aforementioned levels of temperature. From this figure, we notice that the level of central deformation (u_1/L) of the pump actuator decreases with an increase in the temperature irrespective of the applied electric field. From Figure 10, it is also evident that the dimensionless electric field required

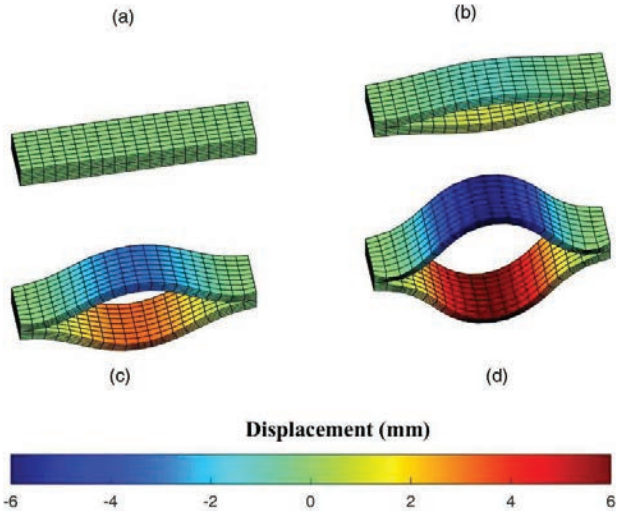

Figure 11 Deformed configurations of a bi-layered buckling pump actuator with a color plot of the deflection (u_1) in mm at different values of applied dimensionless electric field e (a) 0.0, (b) 0.35, (c) 0.6 (d) 0.75, and temperature $\theta = 353$ K.

to trigger the buckling instability increases with an increase in the actuator temperature. Figures 11(a–d) demonstrate the deformed configurations along with displacement contour plots of the buckling pump actuator at the temperature of 353 K, corresponding to the values i.e., 0.0, 0.35, 0.6, and 0.75 of the applied dimensionless electric field. From Figure 11(d), we observe the maximum buckling or deflection of around 5 mm magnitude, when applied electric field is equal to 0.75.

Physically, the increase in temperature increases the number of the microstates, consisting of the elastomer, thereby enhances the entropy and the thermodynamic system approaches the more stabilized equilibrium state. Thus, diminution in the level of deformation of the bending and buckling pump actuators with temperature enhancement is observed.

5 Conclusion

In conclusion, we presented a finite element model for investigating the nonlinear thermo-electromechanical behavior of dielectric elastomer actuators undergoing inhomogeneous deformation during their operation. The accuracy of the developed finite element code was demonstrated by comparing the numerical results with the corresponding analytical solutions

for the well-known pull-in instability of a planar actuator. We investigated the temperature effects on the electro-mechanical actuation response of the bi-layered bending actuator and buckling pump actuator involving inhomogeneous deformation. The numerical results demonstrated an increment in the instability electric field with the temperature rise. The level of deformation of the bi-layered bending actuator and buckling pump actuator for any given level of the applied electric field is found to be decreasing with an increase in the temperature. Future developments may focus on incorporating the viscoelasticity material model in the present finite element framework for assessing the viscoelastic effects on the thermo-electro-mechanical response of inhomogeneously deforming dielectric elastomers. The present work also needs further experimental corroboration.

Acknowledgement

AKS acknowledges the financial support from the Department of Science and Technology (DST), Government of India through Grant No. DST/INSPIRE/04/2019/000500. MMJ acknowledges the financial support provided by the Science and Engineering Research Board (SERB), India through Grant No. EMR/2017/003289.

References

[1] T. Lu, C. Ma, T. Wang, Mechanics of dielectric elastomer structures: A review, Extreme Mechanics Letters 38 (2020) 100752.

[2] P. Lotz, M. Matysek, H.F. Schlaak, Peristaltic pump made of dielectric elastomer actuators, in: Electroactive Polymer Actuators and Devices (EAPAD) 2009, Vol. 7287, International Society for Optics and Photonics, 2009, p. 72872D.

[3] R.E. Pelrine, R.D. Kornbluh, J.S. Eckerle. Elastomeric dielectric polymer film sonic actuator, US patent (2002) 6,343,129.

[4] M. Giousouf, G. Kovacs, Dielectric elastomer actuators used for pneumatic valve technology, Smart Materials and Structures 22(10) (2013) 104010.

[5] A. Khurana, A. Kumar, S.K. Raut, A.K. Sharma, M.M. Joglekar. Effect of viscoelasticity on the nonlinear dynamic behavior of dielectric elastomer minimum energy structures, International Journal of Solids and Structures. (2021);208:141–153.

[6] G. Li, X. Chen, F. Zhou, Y. Liang, Y. Xiao, X. Cao, Z. Zhang, M. Zhang, B. Wu, S. Yin, and Y. Xu, 2021. Self-powered soft robot, Nature 591, no. 7848 (2021): 66–71.

[7] T. Rey, G. Chagnon, J.B. Le Cam, D. Favier. Influence of the temperature on the mechanical behaviour of filled and unfilled silicone rubbers. Polymer Testing. 2013 May 1;32(3):492–501.

[8] Z. Liao, M. Hossain, X. Yao, R. Navaratne, G. Chagnon. A comprehensive thermo-viscoelastic experimental investigation of Ecoflex polymer, Polymer Testing. (2020);86:106478.

[9] Z. Liao, M. Hossain, X. Yao, M. Mehnert, P. Steinmann. On thermo-viscoelastic experimental characterization and numerical modelling of VHB polymer. International Journal of Non-Linear Mechanics. 2020 Jan 1;118:103263.

[10] L. Liu, H. Chen, B. Li, J. Sheng, J. Zhang, C. Zhang, Y. Wang, D. Li, Experimental investigation on electromechanical deformation of dielectric elastomers under different temperatures, Theoretical and Applied Mechanics Letters 5(4) (2015) 155–159.

[11] S. Chen, L. Deng, Z. He, E. Li, G. Li, Temperature effect on the performance of a dissipative dielectric elastomer generator with failure modes, Smart Materials and Structures 25(5) (2016) 055017.

[12] M. Kleo, F. Förster-Zügel, H.F. Schlaak, T. Wallmersperger, Thermo-electro-mechanical behavior of dielectric elastomer actuators: experimental investigations, modeling and simulation, Smart Materials and Structures 29(8) (2020) 085001.

[13] J. Sheng, H. Chen, B. Li, Effect of temperature on the stability of dielectric elastomers, Journal of Physics D: Applied Physics 44(36) (2011) 365406.

[14] J. Sheng, H. Chen, B. Li, Y. Wang, Influence of the temperature and deformation-dependent dielectric constant on the stability of dielectric elastomers, Journal of Applied Polymer Science 128(4) (2013) 2402–2407.

[15] L. Liu, Y. Liu, K. Yu, J. Leng, Thermoelectromechanical stability of dielectric elastomers undergoing temperature variation, Mechanics of Materials 72 (2014) 33–45.

[16] J. Sheng, H. Chen, L. Liu, J. Zhang, Y. Wang, S. Jia, Temperature effects on the dynamic response of viscoelastic dielectric elastomer, Theoretical and Applied Mechanics Letters 3(5) (2013).

[17] R. Vertechy, G. Berselli, V. Parenti Castelli, M. Bergamasco, Continuum thermo-electro-mechanical model for electrostrictive elastomers,

Journal of Intelligent Material Systems and Structures 24(6) (2013) 761–778.
[18] M. Mehnert, M. Hossain, P. Steinmann, On nonlinear thermo-electroelasticity, Proc. R. Soc. A 472 (2190) (2016) 20160170.
[19] V.A. Lubarda, Constitutive theories based on the multiplicative decomposition of deformation gradient: Thermoelasticity, elastoplasticity, and biomechanics, Applied Mechanics Reviews 57(2) (2004) 95–108.
[20] M. Mehnert, M. Hossain, P. Steinmann, Numerical modeling of thermo-electro-viscoelasticity with field-dependent material parameters, International Journal of Non-Linear Mechanics. (2018); 106:13–24.
[21] P. Erbts, S. Hartmann, A. Düster, A partitioned solution approach for electro-thermo-mechanical problems, Archive of Applied Mechanics 85(8) (2015) 1075–1101.
[22] P. Erbts, A. Düster, Accelerated staggered coupling schemes for problems of thermoelasticity at finite strains, Computers & Mathematics with Applications 64(8) (2012) 2408–2430.
[23] A. McBride, S. Bargmann, D. Pond, G. Limbert, Thermoelastic modelling of the skin at finite deformations, Journal of thermal biology 62 (2016) 201–209.
[24] D.S. Malkus, T.J. Hughes, Mixed finite element methods—reduced and selective integration techniques: a unification of concepts, Computer Methods in Applied Mechanics and Engineering 15(1) (1978) 63–81.
[25] A.K. Sharma, M.M. Joglekar, A numerical framework for modeling anisotropic dielectric elastomers, Computer Methods in Applied Mechanics and Engineering 344 (2019) 402–420.
[26] A.K. Sharma, P. Kumar, A. Singh, D.M. Joglekar, M.M. Joglekar, Electromechanical instability of dielectric elastomer actuators with active and inactive electric regions, Journal of Applied Mechanics 86(6) (2019) 061008.
[27] L. Liu, H. Chen, B. Li, Y. Wang, D. Li. Thermal and strain-stiffening effects on the electromechanical breakdown strength of dielectric elastomers. Applied Physics Letters; 107(6) (2015) 062906.
[28] A.K. Sharma, N. Arora, M.M. Joglekar, DC dynamic pull-in instability of a dielectric elastomer balloon: an energy-based approach, Proceedings of the Royal Society of London A: Mathematical, Physical and Engineering Sciences 474 (2018) 2211.
[29] A.K. Sharma, S. Bajpayee, D.M. Joglekar, M.M. Joglekar, Dynamic instability of dielectric elastomer actuators subjected to unequal biaxial prestress, Smart Materials and Structures. 26(11) (2017) 115019.

[30] A.K. Sharma, M.M. Joglekar, Effect of anisotropy on the dynamic electromechanical instability of a dielectric elastomer actuator, Smart Materials and Structures 28(1) (2019) 015006.
[31] A.K. Sharma, N. Sheshkar, A. Gupta, Static and dynamic stability of dielectric elastomer fiber composites, Materials Today: Proceedings 44 (2021) 2043–2047.
[32] A.K. Sharma, M.M. Joglekar, A computationally efficient locking free numerical framework for modeling visco-hyperelastic dielectric elastomers, Computer Methods in Applied Mechanics and Engineering 352 (2019) 625–653.

Biographies

Atul Kumar Sharma obtained his Ph.D. in Mechanical Engineering from Indian Institute of Technology Roorkee, India, in 2019. He is currently an Assistant Professor of Mechanical Engineering at Indian Institute of Technology Jodhpur, India. His research interests are: Mechanics of soft active materials, Finite element methods for coupled field problems, Stability analysis and control of electrically driven mechanical structures, Wave propagation in soft active composite materials, Topology optimization.

Aman Khurana received the bachelor's degree in mechanical engineering from Graphic Era University, Dehradun in 2013, the master's degree in applied mechanics from Motilal Nehru National Institute of technology, Allahabad in 2017, respectively. He is currently working as research scholar at the Department of Mechanical and Industrial Engineering, IIT Roorkee. His research areas include analysis of dielectric elastomer based minimum energy structures, soft-active materials, smart material etc.

Manish M. Joglekar is an Associate Professor at the Department of Mechanical and Industrial Engineering, IIT Roorkee. He obtained his B.E. from Mumbai University, M.E. from Walchand College of Engineering, and PhD from IIT Bombay, all three in Mechanical Engineering discipline. Prior to joining IIT Roorkee as an Assistant Professor in 2012, Manish worked as a Research Scientist at General Motors' India Science Lab in Bengaluru. His broad research interests include computational mechanics, nonlinear elasticity, and structural dynamics. In particular, his research group at IIT Roorkee has been active in addressing the mechanics of soft active materials both theoretically and experimentally, with a specific focus on biomimetic engineering. He has about 40 papers published in various international journals and conferences of repute. Manish is the recipient of the 2018 IIT Roorkee Outstanding Teacher Award and the 2019 Institute Research Fellowship for the Outstanding Young Faculty.